Passive alteration and control of convective heat transfer utilizing alternate porous cavity-block wafers

P. C. Huang and K. Vafai
Department of Mechanical Engineering, The Ohio State University, Columbus, OH, USA

Passive heat-transfer augmentation or alteration along an external boundary using alternately emplaced porous cavity-block wafers is analyzed in this work. The Brinkman-Forchheimer–extended Darcy Model, which accounts for the effects of impermeable boundary and inertia, is used to characterize the flow field inside the porous region. The present work constitutes an innovative way of altering and control of the flow and heat-transfer characteristics of an external surface. The formulation of the problem shows that flow and heat-transfer characteristics depend on seven dimensionless parameters, namely, the Reynolds number, Darcy number, the Prandtl numbers, inertial parameter, two pertinent geometric parameters, and the number of porous cavity-block obstacles. Solution of the governing equations is carried out using the steam function-vorticity formulation, and an in-depth discussion of the results for various physical interactions between the recirculating flows inside of the cavity and the external flow is presented. Several interesting phenomena such as the interactions between the blowing and displacement effects from the porous blocks and the vortices penetrating into the porous cavities are presented and discussed, and it is shown that altering some parametric values can have significant effects on the external momentum and thermal boundary-layer characteristics. The present investigation forms a pertinent and basic research investigation for altering the skin friction and heat-transfer characteristics of an external surface.

Keywords: passive control; porous media; heat transfer alteration

Introduction

Forced convection over external boundaries in the presence of a porous medium has constituted an important area of research for the past several decades. This is due to the very fundamental and generic nature of this type of problem, which makes it pertinent to a wide variety of applications including drying processes, heat pipes, filtration, direct contact heat exchangers, electronic cooling, thermal insulation, and so forth. Tien and Vafai (1989) and Lauriat and Vafai (1991) discuss pertinent aspects of heat transfer in fluid-saturated and unsaturated porous medium as well as various aspects of these applications.

Vafai and Tien (1981) analyzed the effects of a solid boundary and inertial force on flow over an external boundary, after establishing the governing equations by a local volume-averaging technique. They showed that for the flow field the boundary effect is confined within a thin momentum boundary layer, which often plays an insignificant role in the overall flow consideration; however, when the thermal boundary layer's thickness is less than or of the same order as that of the momentum boundary layer, the effect of boundary on the heat transfer is more pronounced. Kaviany (1987) obtained Karman-Pohlhausen solutions for the same flow configuration on the basis of the governing equations developed in Vafai and Tien (1981).

Address reprint requests to Professor Vafai at the Department of Mechanical Engineering, The Ohio State University, Columbus, OH 43210, USA.

Received 18 February 1993; accepted 15 June 1993

An important problem related to forced convection through a porous medium is flow and heat transfer in composite systems. This involves the study of fluid flow above and through a porous medium. The flow over the fluid region is governed by the Navier–Stokes equation, and the flow through the porous medium is governed by the generalized momentum equation, which includes the effects of flow inertia as well as friction caused by macroscopic shear stress (Vafai and Tien 1981). These two flows are coupled through the interface boundary conditions at the porous-fluid interface. The interactions of flow and temperature fields between the porous-saturated region and the fluid region has a significant influence on the convection phenomenon in these systems.

The present work forms a fundamental investigation into the effects of using a combination of porous blocks and embedded porous wafers for altering and controlling the skin friction and heat-transfer characteristics of an external surface. As such, this configuration does present the fundamental characteristics that can apply to various applications related to alteration of flow and heat-transfer characteristics. Variations in skin friction and Nusselt numbers as a result of using these types of structures are analyzed in detail. The present work constitutes an innovative passive method for altering and controlling the flow and heat-transfer characteristics of an external surface.

This type of basic composite system is of importance in various applications such as crude oil extraction, solidification of castings, geothermal operations, nuclear waste repositories, thermal insulation, and so forth. Several investigations were devoted to the problem of finding the proper set of boundary conditions at the interface between a fluid flow in a porous medium and the adjacent region without a porous medium.

Beavers and Joseph (1967) experimentally reported the mass efflux of a Poiseuille flow over a naturally permeable surface based on Darcy's law. They found that when a viscous fluid passes over a porous solid, tangential stress entrains the fluid below the interface with a velocity, which is slightly greater than that of the fluid in the bulk of the porous medium. Levy and Sanchez-Palencia (1975) found that when the typical length scale of the external flow is large compared with the microscopic scale, the velocity field transition at the interface from the porous media to the free fluid region occurs over a thin region of the order of the pore scale. They also showed that depending on the direction of the pressure gradient in the porous medium two different kinds of phenomena may appear at the interface.

More relevant to the present study is the work of Vafai and Thiyagaraja (1987), which was based on the generalized model established in Vafai and Tien (1981). They performed a theoretical analysis for a general class of problems involving interface interactions on the flow and temperature fields for three basic types of interface composites. Vafai and Kim (1990) studied forced convection over an external boundary with a porous substrate. They found that the porous substrate causes a blowing effect on the flow field. They also found that the porous substrate significantly reduces the frictional drag, and it can either enhance or reduce the heat transfer at the wall. Another related problem is the recirculating flow created by boundary layer separation because of an abrupt change in body geometry. Heat transfer in such flows without any porous medium has been reviewed by Fletcher et al. (1974) and Aung and Watkins (1979).

Although there is a large body of literature about transport through porous media, a far more complex problem on transport through porous-fluid structures has received very little attention. In fact, transport through porous substrate cavities or blocks has not been studied except for the present set of investigations. This manuscript provides an in-depth and vivid presentation of the physics and the relevance of using a combination of porous blocks and embedded porous substrates for altering and controlling the flow and temperature fields, and therefore changing the skin friction and heat-transfer characteristics of an external surface. This is done through a detailed analysis and in-depth discussions of the significance of these structures, and their crucial influence on altering the skin friction and heat-transfer characteristics of an external surface using this type of configuration. The present investigation considers the basic and original problem, and it does present several very interesting results.

Analysis of external forced convection in a porous-fluid composite system is significantly more complicated because of the complex geometric configuration of these types of systems. This work presents a numerical study of forced convection over a composite system, which is composed of alternating porous cavity and block regions separated by the exposed areas of the plate. Because little attention has been focused on external forced convection fluid flow and heat transfer in the porous-fluid composite system, the major goal of the present study is to investigate fundamental changes in the flow and temperature fields owing to the existence of cavity-block porous obstacles and the interactions between the blowing and displacement effects from the porous blocks and the vortices

Notation

A	Dimensionless geometric parameter, W^*/H^*
B	Dimensionless geometric parameter, D^*/W^*
D	Spacing between cavities or blocks, m
$\mathrm{Da_L}$	Darcy number, K/L^2
F	A function used in expressing inertia terms
$g(x, y)$	Curve defining the porous/fluid interface
H	Thickness of the porous medium, m
k	Thermal conductivity, W/mK
K	Permeability of the porous medium, m^2
ℓ_1	Length of plate upstream from the first obstacle, m
ℓ_2	Length of plate downstream from the last obstacle, m
L	Length of the external boundary as shown in Figure 1, m
n	Coordinate normal to the porous/fluid interface
N	Number of blocks
P	Pressure, Pa
$\mathrm{Pe_L}$	Peclet number, $u_\infty L/\alpha$
Pr	Prandtl number, v/α
$\mathrm{Re_L}$	Reynolds number, $u_\infty L/v$
t	Coordinate tangential to the porous/fluid interface
T	Temperature, K
u	x-Component velocity, m/s
v	y-Component velocity, m/s
v	Velocity vector, m/s
V	Volume, m^3
W	Width of the porous block, m
x	Horizontal coordinate, m
y	Vertical coordinate, m

Greek symbols

α	Thermal diffusivity, m^2/s
α_{eff}	Effective thermal diffusivity, $k_{\mathrm{eff}}/\rho_{\mathrm{f}}c_{\mathrm{p,f}}$, m^2/s
Δx	x-Direction width of the control volume
Δy	y-Direction width of the control volume
δx	x-Direction distance between two adjacent grid points
δy	y-Direction distance between two adjacent grid points
ϵ	Porosity of the porous medium
θ	Dimensionless temperature, $(T - T_\infty)/(T_\mathrm{w} - T_\infty)$
Λ_L	Inertial parameter, $FL\epsilon/\sqrt{\mathrm{K}}$
μ	Dynamic viscosity, kg/ms
ν	Kinematic viscosity, m^2/s
ξ	Vorticity
ρ	Density, $\mathrm{kg/m}^3$
Φ	Transported property; general dependent variable
ψ	Stream function

Superscripts

*	Dimensionless quantity
f	Fluid

Subscripts

eff	Effective
f	Fluid
P	Porous
∞	Condition at infinity

Other

$\langle\ \rangle$	Local volume average of a quantity
[a, b]	Larger of a and b

penetrating into the porous cavities. Furthermore, the influence of the governing physical parameters is also thoroughly analyzed, and it is shown that altering some parametric values can have significant effects on the external momentum and thermal boundary-layer characteristics.

Analysis

The configuration for the problem under investigation is depicted in Figure 1. The width and height of the rectangular porous cavities and blocks are H and W, respectively, the distance between any given cavity and a block is D, the length of the external boundary L, the steam velocity u_∞, and the free stream temperature is T_∞. The external boundary is maintained at a constant temperature T_w. It is assumed that the flow is steady, laminar, incompressible, and two-dimensional. In addition, the thermophysical properties of the fluid and the matrix are assumed to be constant, and the porous medium is considered homogeneous, isotropic, nondeformable, and in local thermodynamic equilibrium with the fluid. The governing conservation equations for the present problem will be separately written for the porous and fluid regions. Treating the solid matrix and the fluid as a continuum, the local volume averages of the conservation equations for mass, momentum, and energy in the porous region, which account for the effects of the inertial and impermeable boundary, are (Vafai and Tien 1981)

$$\nabla \cdot \langle \mathbf{v} \rangle = 0 \tag{1}$$

$$\left(\frac{\rho_f}{\epsilon}\right)\langle(\mathbf{v}\cdot\nabla)\mathbf{v}\rangle = -\nabla\langle P\rangle^f + \left(\frac{\mu_f}{\epsilon}\right)\nabla^2\langle \mathbf{v}\rangle - \left(\frac{\mu_f}{K}\right)\langle \mathbf{v}\rangle + \left(\frac{\rho_f F \epsilon}{\sqrt{K}}\right)[\langle \mathbf{v}\rangle\cdot\langle \mathbf{v}\rangle]J \tag{2}$$

$$(\langle \mathbf{v}\rangle\cdot\nabla\langle T\rangle) = \alpha_{eff}\nabla^2\langle T\rangle \tag{3}$$

where $\langle\ \rangle$ denotes the local volume average of a quantity, v represents the velocity vector, ρ_f the fluid density, ϵ the porosity, K the permeability, J a unit vector oriented along the velocity vector, $\langle P\rangle^f$ the intrinsic phase average of pressure, μ_f the fluid viscosity, and F is an empirical function that depends primarily on the microstructure of the porous medium.

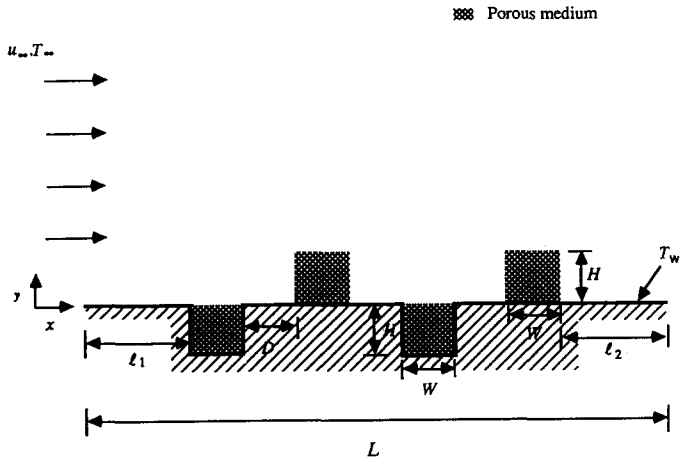

Figure 1 Schematic diagram of flow and heat transfer through alternate porous cavity-block obstacles

The conservation equations for mass, momentum, and energy in the fluid region are

$$\nabla \cdot \mathbf{v} = 0 \tag{4}$$

$$\mathbf{v}\cdot\nabla\mathbf{v} = -\frac{1}{\rho_f}\nabla P + \nu_f\nabla^2\mathbf{v} \tag{5}$$

$$\mathbf{v}\cdot\nabla T = \alpha_f\nabla^2 T \tag{6}$$

The associated boundary conditions necessary to complete the formulation of the problem are

$$u = u_\infty, v = 0, P = P_\infty, T = T_\infty \quad \text{at } x = 0 \tag{7}$$

$$u = \langle u\rangle = 0, v = \langle v\rangle = 0, T = \langle T\rangle = T_w \quad \text{on the solid wall} \tag{8}$$

$$u = u_\infty, P = P_\infty, T = T_\infty \quad \text{as } y \to \infty \tag{9}$$

In addition these two sets of conservation equations are coupled by the following matching conditions at the porous-fluid interface, which satisfy the continuity of the velocity, pressure, stress, temperature, and heat flux across the interface,

$$\langle u\rangle_{g(x,y)=0} = u|_{g(x,y)=0}, \langle v\rangle|_{g(x,y)=0} = v|_{g(x,y)=0} \tag{10a}$$

$$\langle P\rangle|_{g(x,y)=0} = P|_{g(x,y)=0}, \mu_{eff}\left.\frac{\partial\langle v\rangle}{\partial n}\right|_{g(x,y)=0} = \mu_f\left.\frac{\partial v}{\partial n}\right|_{g(x,y)=0} \tag{10b}$$

$$\mu_{eff}\left(\frac{\partial\langle u\rangle}{\partial n} + \frac{\partial\langle v\rangle}{\partial t}\right)\Bigg|_{g(x,y)=0} = \mu_f\left(\frac{\partial u}{\partial n} + \frac{\partial v}{\partial t}\right)\Bigg|_{g(x,y)=0} \tag{10c}$$

$$\langle T\rangle|_{g(x,y)=0} = T|_{g(x,y)=0}, k_{eff}\left.\frac{\partial\langle T\rangle}{\partial n}\right|_{g(x,y)=0} = k_f\left.\frac{\partial T}{\partial n}\right|_{g(x,y)=0} \tag{10d}$$

where $g(x, y) = 0$ is the curve defining the porous-fluid interface. The derivative with respect to n and t represents the normal and tangential gradients, respectively, to the curve $g(x, y) = 0$ at any point on the interface. It should be noted that here we are not trying to resolve a philosophical question with respect to the physical nature of the interface or the micromechanics of a porous-fluid interface but rather use the established and classical form of the interface conditions (Vafai and Kim 1990). To accommodate the solution of the transport equation in both fluid and porous regions, the effective viscosity that refers to the coefficient in front of the Laplacian of the velocity in Equation 2 of the fluid-saturated porous medium is set equal to the fluid viscosity. It has been found that this approximation provides a good agreement with experimental data (Lundgren 1972; Neale and Nader 1984). Introducing the stream function and vorticity as

$$u = \langle u\rangle = \frac{\partial\psi}{\partial y}, v = \langle v\rangle = -\frac{\partial\psi}{\partial x} \tag{11}$$

$$\xi = \frac{\partial v}{\partial x} - \frac{\partial u}{\partial y} = \frac{\partial\langle v\rangle}{\partial x} - \frac{\partial\langle u\rangle}{\partial y} \tag{12}$$

these two sets of conservation equations are transformed into one set of dimensionless stream function-vorticity formulation, which is valid throughout the composite system.

$$\frac{\partial\psi^*}{\partial y^*}\frac{\partial\xi^*}{\partial x^*} - \frac{\partial\psi^*}{\partial x^*}\frac{\partial\xi^*}{\partial y^*} = \frac{1}{Re_L}\nabla^2\xi^* + S^* \tag{13}$$

$$\nabla^2\psi^* = -\xi^* \tag{14}$$

$$\frac{\partial\psi^*}{\partial y^*}\frac{\partial\theta}{\partial x^*} - \frac{\partial\psi^*}{\partial x^*}\frac{\partial\theta}{\partial y^*} = \nabla\cdot\left(\frac{1}{Pe_L}\nabla\theta\right) \tag{15}$$

the nondimensional parameters in the fluid region are

$$\mathrm{Re}_L = \frac{u_\infty L}{\nu_f}, \mathrm{Pe}_L = \frac{u_\infty L}{\alpha_f}, S^* = 0 \tag{16a}$$

and in the porous region the nondimensional parameters are

$$\mathrm{Pe}_L = \frac{u_\infty L}{\alpha_{\mathrm{eff}}}, \mathrm{Da}_L = \frac{K}{L^2}, \Lambda_L = \frac{FL\epsilon}{K^{1/2}} \tag{16b}$$

and

$$S^* = -\frac{1}{\mathrm{Re}_L \mathrm{Da}_L}\xi^* - \Lambda_L|v^*|\xi^* - \Lambda_L\left(v^*\frac{\partial|v^*|}{\partial x^*} - u^*\frac{\partial|v^*|}{\partial y^*}\right) \tag{17}$$

Here S^* can be considered as the term that contributes to the vorticity generation because of the presence of the porous medium. This source term is zero in the fluid region as can be seen by examining Equation 5. However, the source term is nonzero and given by Equation 17 for the porous region. In addition, the dimensionless boundary conditions are

$$\psi^* = y^*, \xi^* = -\frac{\partial^2\psi^*}{\partial x^{*2}}, \theta = 0, \text{ at } x^* = 0 \tag{18}$$

$$\psi^* = 0, \xi^* = -\frac{\partial^2\psi^*}{\partial x^{*2}}, \theta = 1, \text{ at}$$

$$x^* = \begin{cases} \ell_1^* + 2(N-1)(W^* + D^*) \\ \ell_1^* + W^* + 2(N-1)(W^* + D^*) \end{cases}, 0 > y^* > -H^* \tag{19}$$

and

$$\psi^* = 0, \xi^* = -\frac{\partial^2\psi^*}{\partial y^{*2}}, \theta = 1, \text{ at}$$

$$x^* = \left\{\begin{array}{l} \ell_1^* + 2(N-1)(W^* + D^*) < x^* < \ell_1^* + W^* \\ \quad + 2(N-1)(W^* + D^*), \quad y^* = -H^* \\ 0 < x^* < \ell_1^* \\ \ell_1^* + W^* + 2(N-1)(W^* + D^*) < x^* < \ell_1^* \\ \quad + 2N(W^* + D^*) \\ (1 - \ell_2^*) < x^* < 1 \end{array}\right\} y^* = 0 \tag{20}$$

and

$$\frac{\partial\psi^*}{\partial y^*} = 1, \xi^* = -\frac{\partial^2\psi^*}{\partial x^{*2}}, \theta = 0, \text{ as } y^* \to \infty \tag{21}$$

where $N(= 1, 2, \ldots)$ is the number of the porous cavity-block composites. The dimensionless variables in the above equations are defined as follows:

$$x^* = \frac{x}{L}, y^* = \frac{y}{L}, u^* = \frac{u^*}{u_\infty}, v^* = \frac{v}{u_\infty}, |v^*| = \sqrt{u^{*2} + v^{*2}} \tag{22a}$$

$$\psi^* = \frac{\psi}{u_\infty L}, \xi^* = \frac{L\psi}{u_\infty}, \theta = \frac{T - T_\infty}{T_w - T_\infty} \tag{22b}$$

$$H^* = \frac{H}{L}, \ell_1^* = \frac{\ell_1}{L}, \ell_2^* = \frac{\ell_2}{L}, D^* = \frac{D}{L}, W^* = \frac{W}{L} \tag{22c}$$

Based on the preceding equations, boundary conditions, and geometrical arrangement of porous cavities and blocks, it is seen that the present problem is governed by seven dimensionless parameters. These are the Darcy number, Reynolds number, two Prandtl numbers, inertia parameter, geometrical parameters A and B, and the number of cavities N, where

$$A = \frac{W^*}{H^*}, B = \frac{D^*}{W^*} \tag{23}$$

Numerical scheme

To obtain the solution of the foregoing system of equations, the region of interest is overlaid with a variable grid system as shown in Figure 2a. Applying the central differencing for the diffusion terms and the second upwind differencing for the convective terms, the finite-difference form of the vorticity transport, stream function, and energy equations were derived by control-volume integration of these differential equations over discrete cells surrounding grid points, as shown in Figure 2b. This results in a system of equations of the following form

$$C_C\Phi_C = C_N\Phi_N + C_S\Phi_S + C_E\Phi_E + C_w\Phi_W + S^\Phi \tag{24}$$

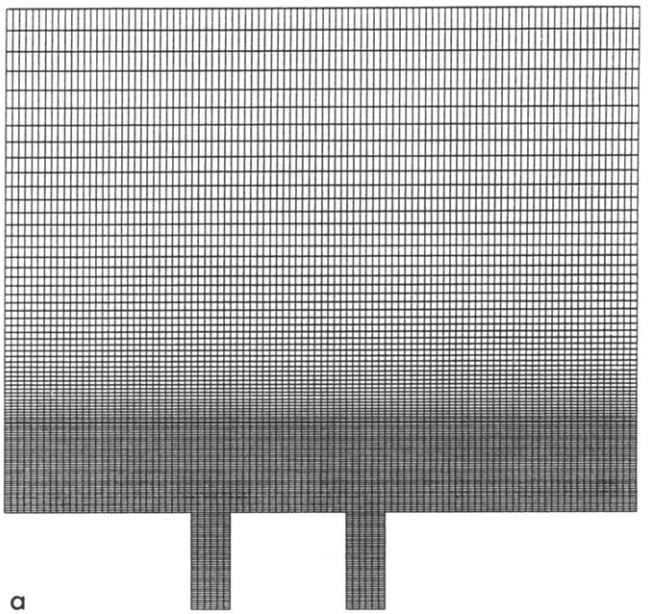

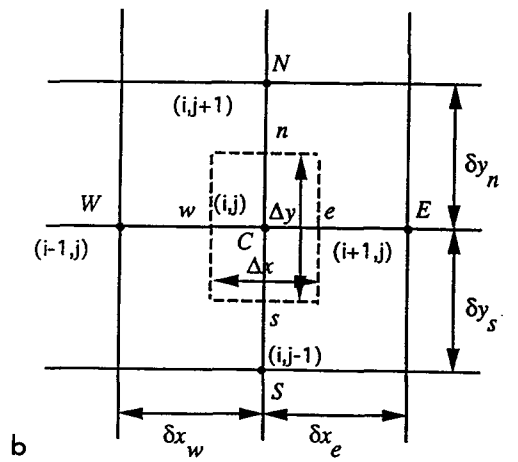

Figure 2 (a) Grid system for the computational domain; and (b) local integration cell

where Φ stands for the transport variables, Cs are coefficients combining convective and diffusive terms, and S^{Φ} is the appropriate source term. The subscripts on C denote the main grid points surrounded by the four neighboring points denoted as N, S, E and W. The finite difference equations for ξ^*, ψ^*, and θ obtained in this manner were solved by the extrapolated-Jacobi scheme. This iterative scheme is based on a double-cyclic routine, which translates into a sweep of only half of the grid points at each iteration step (Adams and Ortega 1982). In solving the finite-difference equations the following convergence criteria was satisfied:

$$\max \left| \frac{\varphi_{i,j}^{n+1} - \varphi_{i,j}^{n}}{\varphi_{i,j}^{n}} \right| < 10^{-6} \tag{25}$$

where φ stands for ξ^*, ψ^*, or θ and n denotes the iteration number.

The treatment of the vorticity at sharp corners requires careful consideration. Several methods of handling this corner vorticity are discussed in Roache (1982). Here to model properly the mathematical limit of a sharp corner, the method of average vorticity values is used (Greenspan 1969). The bifurcation of the vorticity at the corners is essentially handled through the introduction of two different vorticity values. These are ξ_a^* and ξ_b^*, where both are evaluated by using the no-slip wall equation, but ξ_a^* is evaluated by considering the corner being part of the horizontal wall, whereas ξ_b^* is evaluated by considering it to be part of the vertical section of the cavity. Then a single corner vorticity equal to the average of two wall values is obtained.

The interfacial properties play an important role on the porous-fluid system. This is due to the discontinuity of thermophysical properties, such as the permeability, porosity, and thermal conductivity, across the interface. All of these effects on the porous-fluid interface are summarized in the non-dimensional parameter $\mathrm{Da_L}$, Λ_L, and Pr. To obtain a generalized formulation for the entire composite layer Λ_L and $\mathrm{Da_L}$ are taken in general to be variables. This is because the harmonic mean formulation suggested by Patankar (1980) was used to handle the abrupt variation of thermophysical properties such as the permeability and the thermal conductivity across the interface. This ensured the continuity of the convective and diffusive fluxes across the interface without requiring an excessively fine grid. Therefore, in the generalized formulation for the entire composite layer, to preserve all of the interface boundary conditions we must treat Λ_L and $\mathrm{Da_L}$ as variables as explained in Huang and Vafai (1993). This procedure was checked on several available simplified exact and numerical solutions such as those in Vafai and Thiyagaraja (1987) and Poulikakos and Kazmierczak (1987). For the present case $\mathrm{Da_L}$, Λ_L, and Pr at the interface of a control volume are as follows:

$$\mathrm{Da_{L_I}} = \frac{2\mathrm{Da_{L_{eff}}}\mathrm{Da_{L_f}}}{\mathrm{Da_{L_{eff}}} + \mathrm{Da_{L_f}}}, \Lambda_{L_I} = \frac{2\Lambda_{L_{eff}}\Lambda_{L_f}}{\Lambda_{L_{eff}} + \Lambda_{L_f}}, \mathrm{Pr}_I = \frac{2\mathrm{Pr_{eff}}\mathrm{Pr_f}}{\mathrm{Pr_{eff}} + \mathrm{Pr_f}} \tag{26}$$

where the subscripts eff, f, and I stand for effective, fluid, and interfacial, respectively. Therefore, instead of the source terms in Equations 16 and 17, the following source terms were used across the interface:

$$S^* = \frac{u^*}{\mathrm{Re_L}} \frac{\partial}{\partial y^*}\left(\frac{1}{\mathrm{Da_L}}\right) - \frac{v^*}{\mathrm{Re_L}} \frac{\partial}{\partial x^*}\left(\frac{1}{\mathrm{Da_L}}\right) + |v^*| v^* \frac{\partial}{\partial y^*}(\Lambda_L) - |v^*| v^* \frac{\partial}{\partial x^*}(\Lambda_L) \tag{27}$$

$$S^* = -\frac{1}{\mathrm{Re_L Da_L}} \xi^* - \Lambda_L |v^*| \xi^* - \Lambda_L \left(v^* \frac{\partial |v^*|}{\partial x^*} - u^* \frac{\partial |v^*|}{\partial y^*} \right) + \frac{u^*}{\mathrm{Re_L}} \frac{\partial}{\partial y^*}\left(\frac{1}{\mathrm{Da_L}}\right) - \frac{v^*}{\mathrm{Re_L}} \frac{\partial}{\partial x^*}\left(\frac{1}{\mathrm{Da_L}}\right) + |v^*| u^* \frac{\partial}{\partial y^*}(\Lambda_L) - |v^*| v^* \frac{\partial}{\partial x^*}(\Lambda_L) \tag{28}$$

where Equation 27 was used for the fluid, and Equation 28 was used for the porous region. Note that constant values of $\mathrm{Da_L}$, and Λ_L were used for a specified porous substrate.

A nonuniform grid system with a large concentration of nodes in regions of steep gradients, such as the wall, corners, and blocks, was employed. Figure 2a depicts the nonuniform grid system for the computational domain. A very careful analysis was made to ensure grid independence, and the upper boundary was systematically increased until it would have no detectable effect on the results. Three sets of grid systems, 162 × 136, 162 × 195, and 202 × 292 were investigated in this work. It was found that for the most extreme cases there was only less than 1 percent difference in the values of the streamlines and isotherms between the 162 × 195, and 202 × 292 grid systems. Therefore, a 162 × 195 grid system was adopted for the present work.

In this study the computational domain was always chosen to be larger than the physical domain. Along the x-direction, the computational domain starts at a distance one fifth the total length upstream of the physical domain. This procedure eliminates the errors associated with the singular point at the leading edge of the composite system. On the other side, the computational domain is extended over a distance two fifths the total length downstream from the trailing edge of the physical domain. Because the present problem has a significant parabolic character, the downstream boundary condition on the computational domain does not have much influence on the physical domain. The application of the boundary condition at infinity at a finite distance from the wall was also given careful consideration. This was done through the following procedure.

The length of the computational domain in the vertical direction was systematically increased until the maximum vorticity changes for two consecutive runs would become less than 1 percent. In the y-direction the computational domain is extended up to a distance sufficient enough to ensure that even for the smallest value of the Reynolds number the upper boundary lies well outside the boundary layer through the entire domain. In the present study, locating the upper boundary at a distance of eight times the depth of the cavity has been found to be sufficient. Extensions beyond eight times the depth of the cavity had no effect on the solution. We ran extensive tests on the effect of varying the size of the computational domain and observing its effects on the physical domain to ensure that the boundary conditions on the downstream side of the computational domain (the right-hand side) had no influence on our results. In our work for simplicity the conditions at the last interior grid points from the outflow boundary condition in the previous iteration were used and yielded the same solution for the domain of interest except for the region very close (this is the region that was part of our computational domain but not the physical domain) to the downstream boundary as when the other conditions were used.

To validate the numerical scheme used in the present study further, initial calculations were performed for laminar flow over a flat plate (i.e., $H^* = 0$, for no porous substrate) and that over a flat plate embedded in a porous medium (i.e., $H^* \to \infty$ and $W^* \to \infty$) representing the full porous medium case. The

results for $H^* = 0$ agree to better than 1 percent with boundary layer similarity solutions for velocity and temperature fields. The results for $H^* \to \infty$ and $W^* \to \infty$ agree extremely well with data reported by Vafai and Thiyagaraja (1987). These comparisons were found to be similar to those presented in Vafai and Kim (1990).

Results and discussion

The dimensionless parameters that need to be specified for this system are Re_L, Da_L, Λ_L, Pr, A, B, and N. Because these seven basic dimensionless parameters are required to characterize the system, a comprehensive analysis of various combinations of these parameters was done. The results given in this work present only a small fraction of the cases that were investigated. The displayed results were chosen to represent the most pertinent effects of these parameters. In addition, to illustrate the flow and temperature fields better, only the portion that concentrates on the porous-fluid region and its close vicinity are presented. However, the much larger domain was always used for numerical calculations and interpretation of the results.

The range of Reynolds numbers used in the present investigation were chosen such that the laminar conditions prevail. Furthermore, a careful study was done to observe when the turbulent effects become important. The turbulent features appear for Reynolds numbers significantly larger than $Re = 3 \times 10^5$, which is the highest Reynolds number used in the present work. In fact this is one of the advantages of these types of porous obstacles. Had, for example, solid blocks been used instead of porous blocks we would get separation and appearance of turbulence features at much smaller Reynolds numbers (Huang and Vafai 1993).

The influence of the cavity-block structure on the flow field is depicted in Figure 3a for a case where the Reynolds number is 3×10^5, the Darcy number is 8×10^{-6}, the inertial number is 0.35, the dimensionless height and width of the porous cavity or the block are 0.02 and 0.06, respectively, and the dimensionless spacing between the porous cavities and the blocks is 0.06. It can be seen that the streamlines are considerably distorted because of the presence of the porous cavity-block structure. The streamlines move upward while piercing into the porous block and become sparser after passing through it. Physically, this is due to the relatively larger resistance that the flow encounters in the porous block, which in turn displaces the fluid by blowing it from the porous region into the fluid region and reduces mass flow rate through the porous blocks. This effect is more pronounced for the cases with smaller Darcy number or larger inertial number.

Figure 3a also displays a laminar vortex contained within each cavity. The intensity of the eddies within each cavity decreases along the flow direction. These vortices are formed as a result of the entrapped flow striking on the downstream cavity wall and then flowing toward the bottom surface. Because of an increase in the thickness of the external boundary layer along the plate, the mass flow rate penetrating into the subsequent cavity decreases, which, in turn, reduces the intensity of vortex in the cavities along the flow direction. The small fluctuations of streamlines close to the inlet of porous

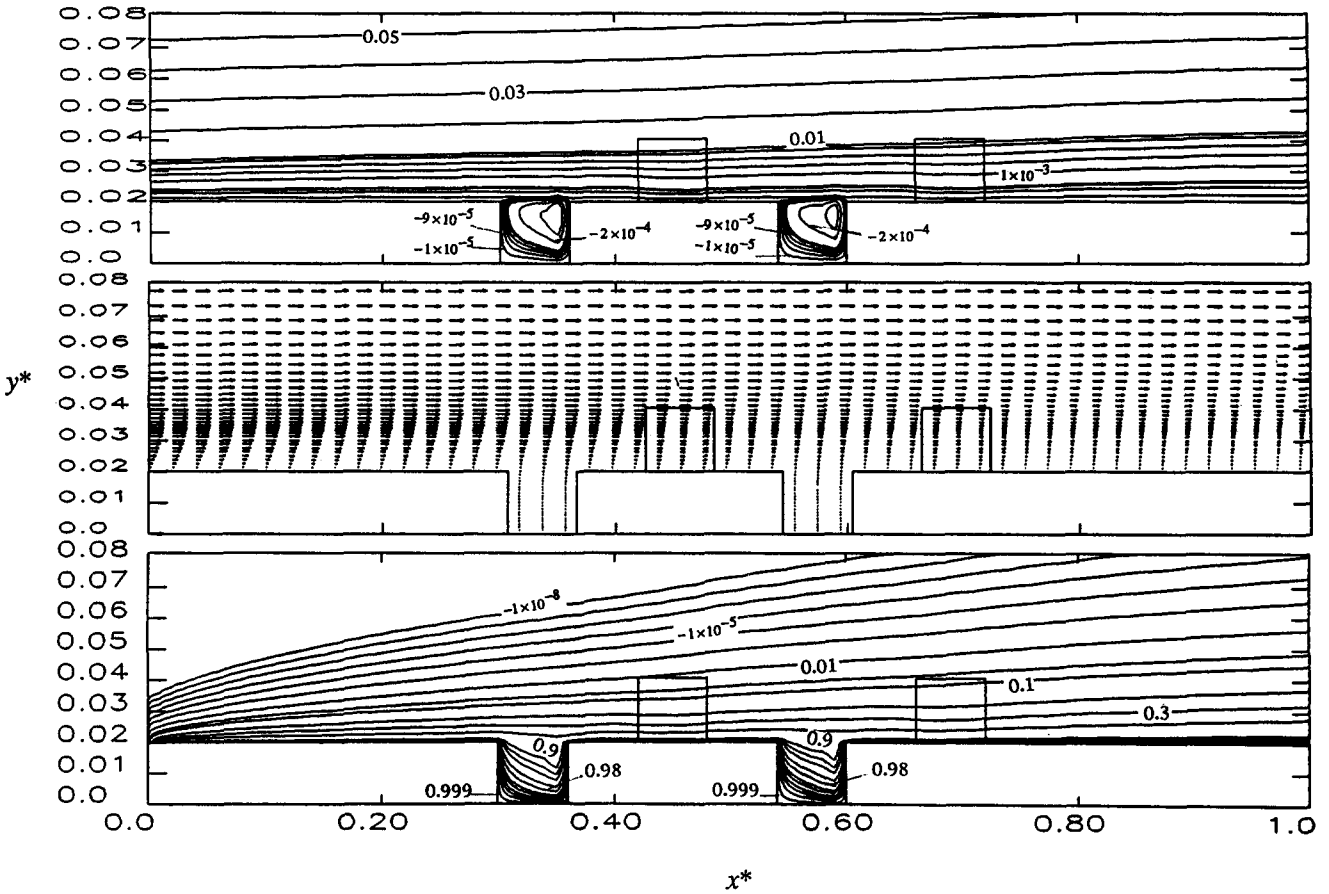

Figure 3 (a) Streamlines; (b) velocity distribution; and (c) isotherms for flow through alternate porous cavity-block obstacles for $Re_L = 3 \times 10^4$, $Da_L = 8 \times 10^{-6}$, $\Lambda_L = 0.35$, $A = 3$, $B = 1$, and $H^* = 0.02$

cavities is due to the macroscopic shear frictional resistance at the porous-fluid interface.

The previously described flow field can also be observed by the velocity field shown in Figure 3b. After the primary flow field encounters the porous blocks, two momentum boundary layers are formed. One layer is along the impermeable wall, and the other is on top of the porous obstacles. Inside of the porous media, as the normal coordinate increases the velocity distribution increases from zero to a constant value, which is maintained until the outer boundary layer appears. The velocity distribution goes through a smooth transition once it crosses the porous-fluid interface and finally approaches a free-stream value. As expected, both momentum boundary layers grow in the streamwise coordinate. Consequently, in the porous region the magnitude of the interfacial velocity decreases to adapt this growth, resulting in a further increase in the thickness of the boundary layer near the wall. These characteristics are consistent with those found in the work of Vafai and Kim (1990). The flow patterns, including the shape of boundary layer, the blowing effect, and the interaction between the recirculating flow inside the cavity and the external flow play a significant role in affecting the temperature field.

Figure 3c shows isotherms corresponding to the flow field shown in Figures 3a, b. There is only one thermal boundary layer and there is little distortion of the temperature field over the flat wall. Inside of the cavities, spacing between isotherms close to the left wall is larger than that close to the right wall. This is due to the larger convective energy transport over the downstream wall of the cavity compared with the one upstream.

Effect of the Darcy number

The Darcy number is directly related to the permeability of the porous medium. To investigate the effect of Darcy number on flow and temperature fields, computations were carried out at $Da_L = 8 \times 10^{-6}$, 4×10^{-7}, 2×10^{-7}, and 1×10^{-7} for $H/L = 0.02$, $A = 3$, $B = 1$, $Re_L = 3 \times 10^5$ and $\Lambda_L = 0.35$. Results of the computations for streamlines and isotherms are presented in Figures 4 and 5. The flow fields displayed in

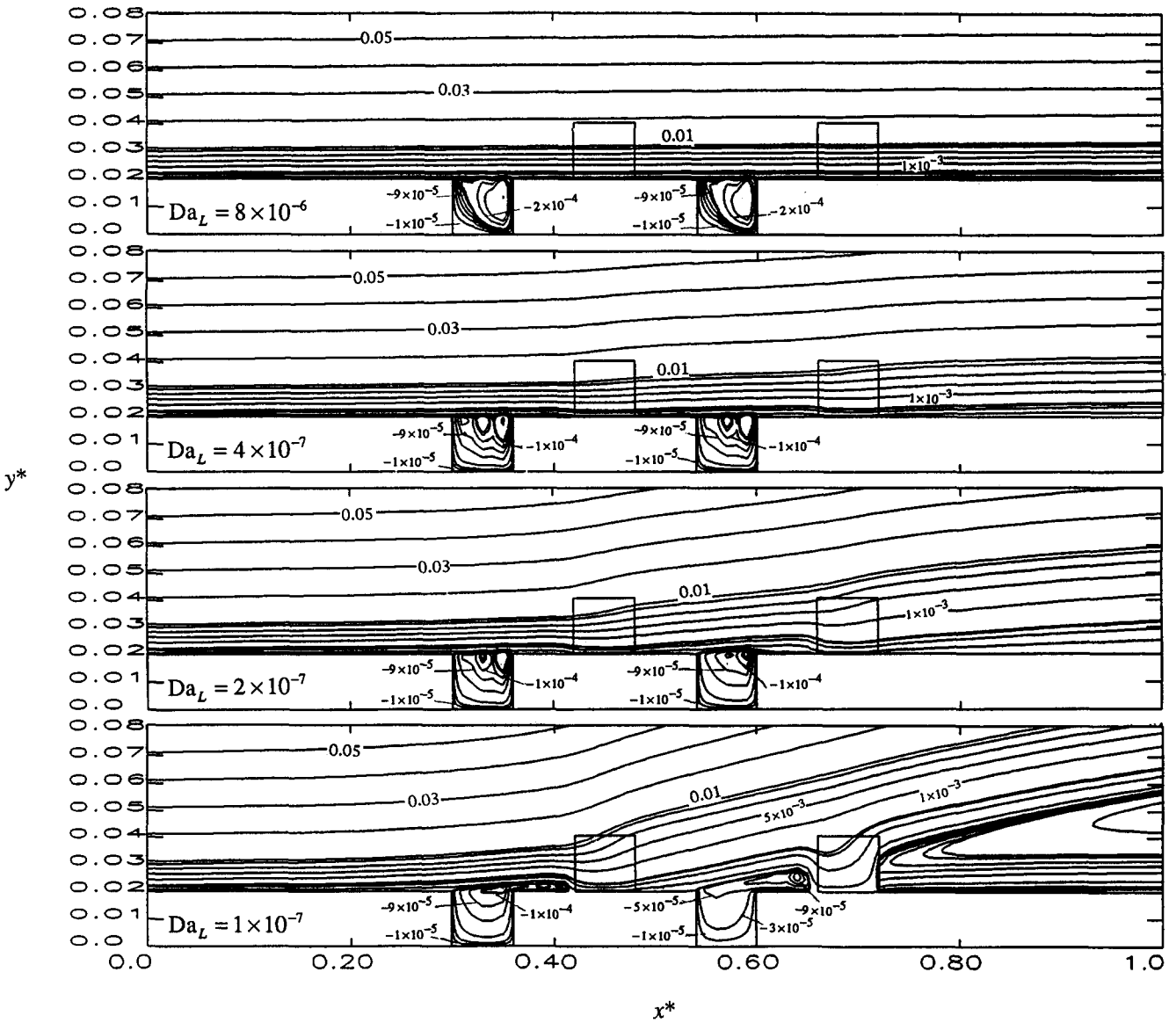

Figure 4 Effects of the Darcy number on streamlines for flow through alternate porous cavity-block obstacle for $Re_L = 3 \times 10^5$, $\Lambda_L = 0.35$, $A = 3$, $B = 1$, $H^* = 0.02$

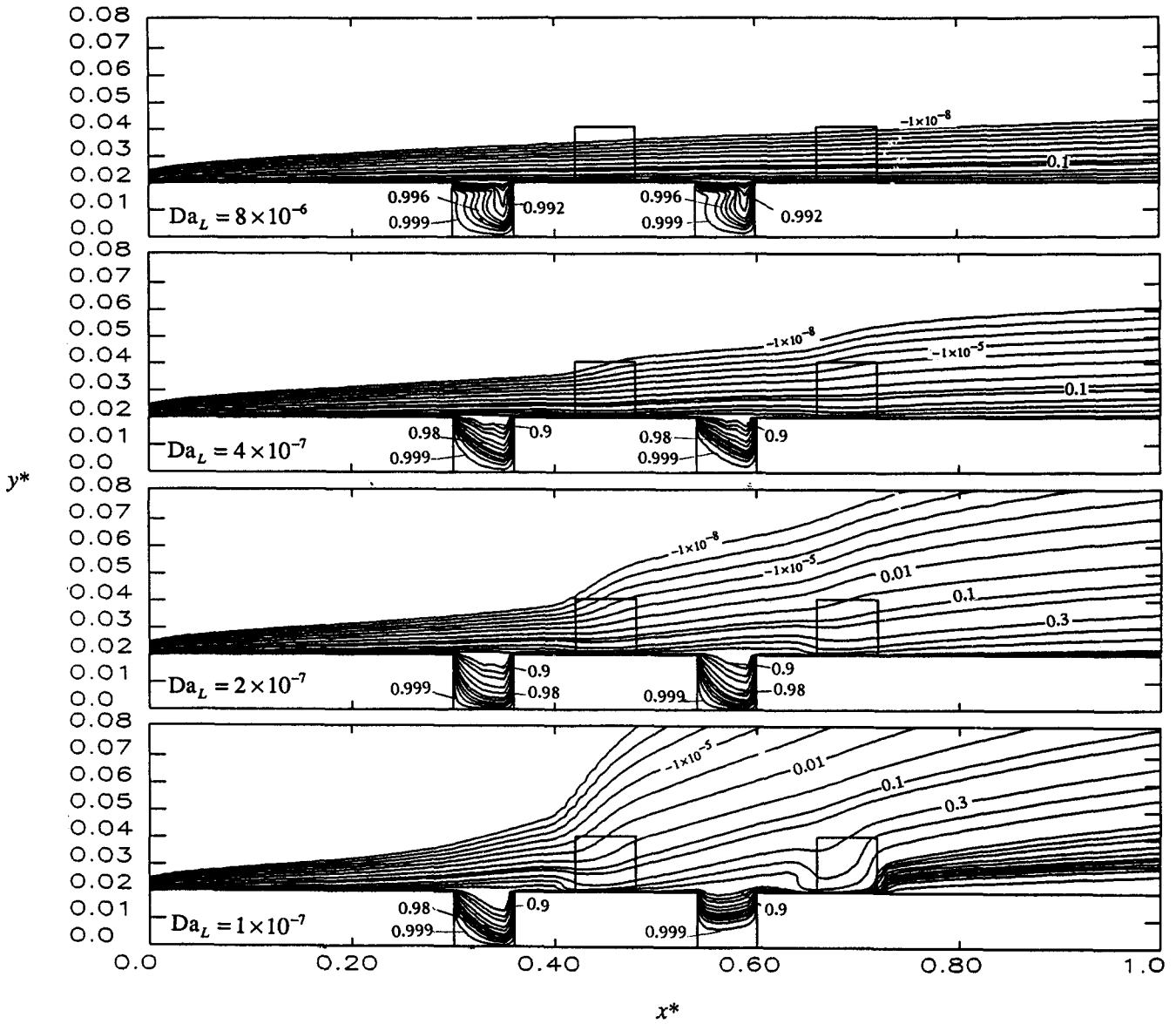

Figure 5 Effects of the Darcy number on isotherms for flow through alternate porous cavity-block obstacles for $Re_L = 3 \times 10^5$, $\Lambda_L = 0.35$, $Pr = 0.7$, $k_{eff}/k_f = 1.0$, $A = 3$, $B = 1$, $H^* = 0.02$

Figures 4a–d reveal that as the Darcy number decreases, the interaction between the vortex inside the cavity and the external flow becomes more pronounced. This is due to the larger bulk frictional resistance to the flow within the porous block for the smaller Darcy number, which, in turn, results in a larger adverse pressure gradient for the porous obstacle. Consequently, the flow rate near the wall is decreased because of the viscous shear stress and the adverse pressure gradient. This results in the formation of a separation zone before the porous block.

For the case of lower Darcy numbers, the larger bulk frictional resistance reduces the mass flow rate perforating into the cavity, causing the uplifting of the streamlines from the base of the cavity. Consequently, an intricate eddy region is formed at the inlet of the porous-fluid interface. For Darcy numbers below 2×10^{-7}, the vortex region in front of the porous blocks gradually becomes part of the recirculating flow inside of the cavities. For low Darcy numbers, the strength of the laminar eddies in the separation zone before the porous blocks, are damped out by the porous matrix frictional resistance, which allows the boundary layer to reattach itself to the wall and form a closed vortex region. Furthermore, for low Darcy numbers, the boundary layer, separation zone, or vortex region covering the inlet of cavities creates a complicated recirculating flow inside the cavities, as seen in Figure 4.

The temperature distribution corresponding to the flow field shown in Figure 4 is displayed in Figure 5. The temperature fields shown in Figure 5 correspond to a case in which the Prandtl number is 0.7, and the conductivity of porous media is equal to that of the fluid. For smaller Darcy numbers, the larger separation zone after the porous cavities increases the distortion of the isotherms near the heated wall. It can be seen that as the Darcy number decreases the thickness of the external boundary layer increases. Initially, as the Darcy number decreases (up to $Da_L = 2 \times 10^{-7}$), the thermal penetration into the cavities increases, especially within the left half section of the cavity. This is the result of the relative increase in the thermal diffusion compared to convection within

the porous medium. The thermal penetration ceases to propagate further into the cavity for Darcy numbers less than 2×10^{-7} because of the aforementioned formation of the intricate eddy region at the inlet of the porous-fluid interface. It should be noted that as the Darcy number is reduced below 1×10^{-7}, an almost stagnant region is formed at the inlet of the cavities. The previously described effects lead to the skin friction and Nusselt number distributions shown in Figure 6.

Effects of the Reynolds number

The effect of an increase or decrease in the Reynolds number is shown in Figures 7 and 8 for $Da_L = 8 \times 10^{-6}$, $\Lambda_L = 0.35$, $Pr = 0.7$, $A = 3$, and $B = 1$ for $Re_L = 3 \times 10^5$, 3×10^4, 1×10^4, and 5×10^3, respectively. Comparison of the streamlines in Figure 7 shows that as the Reynolds number decreases, the distortion of streamlines and boundary layer thickness along the wall becomes more significant. In addition, the center of the vortex for each cavity moves further to the center. This is caused by a reduction in the magnitude of the inertial forces at a lower Reynolds number, thus reducing the penetration extent of the flow into the porous blocks and cavities. This results in a larger blowing effect over the porous block resulting in a larger thickness of boundary layer near the wall. For larger Reynolds numbers, the external flow basically skims past the cavity without a strong interaction with the flow inside of the cavities. However, there is a significant effect on the porous-fluid interface structure at larger Reynolds number.

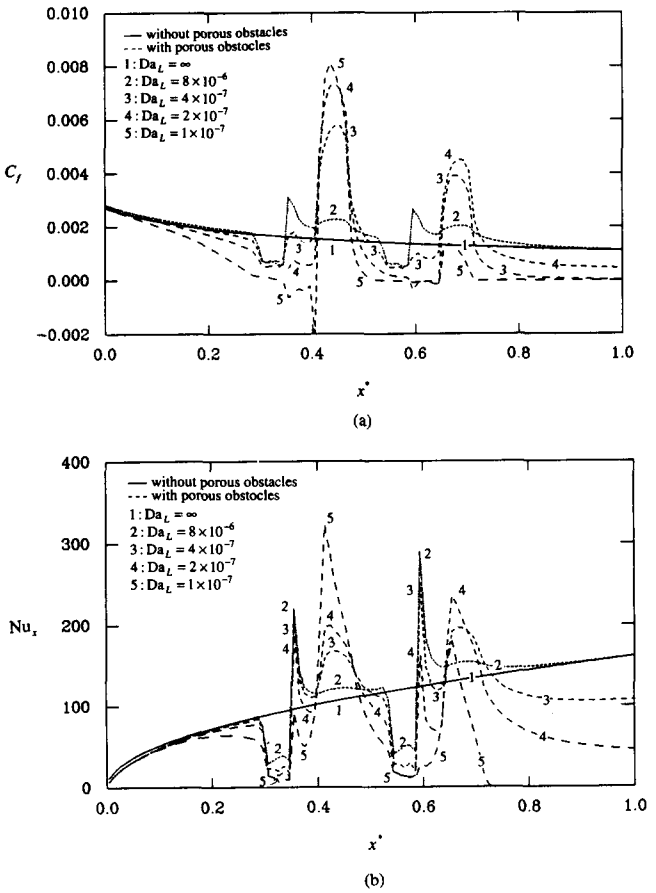

Figure 6 Effects of the Darcy number on (a) friction coefficient and (b) Nusselt number for flow through alternate porous cavity-block obstacles for $Re_L = 3 \times 10^5$, $\Lambda_L = 0.35$, $Pr = 0.7$, $k_{eff}/k_f = 1.0$, $A = 3$, $B = 1$, $H^* = 0.02$

The previously cited distortion of the flow field leads to the skin friction and Nusselt number distributions shown in Figure 8. The distortions and variations of the skin friction and Nusselt number distributions are direct result of the described flow field.

Inertial effects

The inertial effects become significant for the higher permeability and the lower fluid viscosity (Vafai and Tien 1981). Figures 9 and 10 show the effect of the inertial parameter on the flow field and the skin friction and Nusselt number distributions for $Re_L = 3 \times 10^5$, $Da_L = 8 \times 10^{-6}$, $Pr = 0.7$, $A = 3$, and $B = 1$, for $\Lambda_L = 0.35$, 35, 70, and 210, respectively. As expected, the distortion of the streamlines and isotherms and the size of the vortices near the wall increase with an increase in the inertial parameter. This is the result of the larger bulk frictional resistance that the flow encounters at larger values of the inertial parameter. This, in turn, leads to a larger blowing effect, which reduces the mass flow rate through the porous media, and results in a larger adverse pressure gradient in front of the porous obstacles, creating a larger separation zone.

Prandtl number effects

To investigate the effect of the Prandtl number on the flow and the Nusselt number distribution, three different Prandtl numbers were chosen such that they will cover a wide range of thermophysical properties. The numerical results are presented in Figures 11 and 12 for $Re_L = 3 \times 10^5$, $Da_L = 8 \times 10^{-6}$, $\Lambda_L = 0.35$, $A = 3$, and $B = 1$ for three different fluids with $Pr = 0.7$ (air), $Pr = 7$ (water), and $Pr = 100$ (a representative oil), respectively. Obviously, the variations of Prandtl number have no effect on the flow field, and therefore the flow field is the same for all Prandtl numbers. This flow field is shown in Figure 11a. As seen in Figures 11b–d, because of the lower value of the thermal diffusivity relative to the momentum diffusivity the extent of the thermal penetration over the external boundary as well as into the cavity becomes significantly confined for larger values of Prandtl numbers. These effects are reflected in the Nusselt number distributions shown in Figure 12.

Effect of the first geometric parameter A

The first geometric parameter $A = W^*/H^*$ represents the influence of the geometry of the porous obstacles on the flow. For this purpose, two configurations have been investigated. Figures 13 and 14 show the streamlines and isotherms for $Re_L = 3 \times 10^5$, $Da_L = 8 \times 10^{-6}$, $\Lambda_L = 0.35$, $Pr = 0.7$, and $B = 1$ for these two cases corresponding to $A = 3$ and 4, respectively. It should be noted that Figures 13 and 14 also represent the effects of the variations of the second geometric parameter B, which is to be discussed later. Comparison of Figures 13 and 14 shows that as the value of A increases, the distortion in streamlines and isotherms become more pronounced. Moreover, for larger values of A, the boundary layer separation zone in front of the porous block increases, which, in turn, affects the flow and temperature fields inside of the cavities. This is a direct result of the relative increase in the length of the porous block, which extends the blowing action, and subsequent deceleration of the flow field.

Effect of the second geometric parameter B

The effect of interspacing between a porous cavity and a porous block ($B = D^*/W^*$) were studied for two cases. These cases

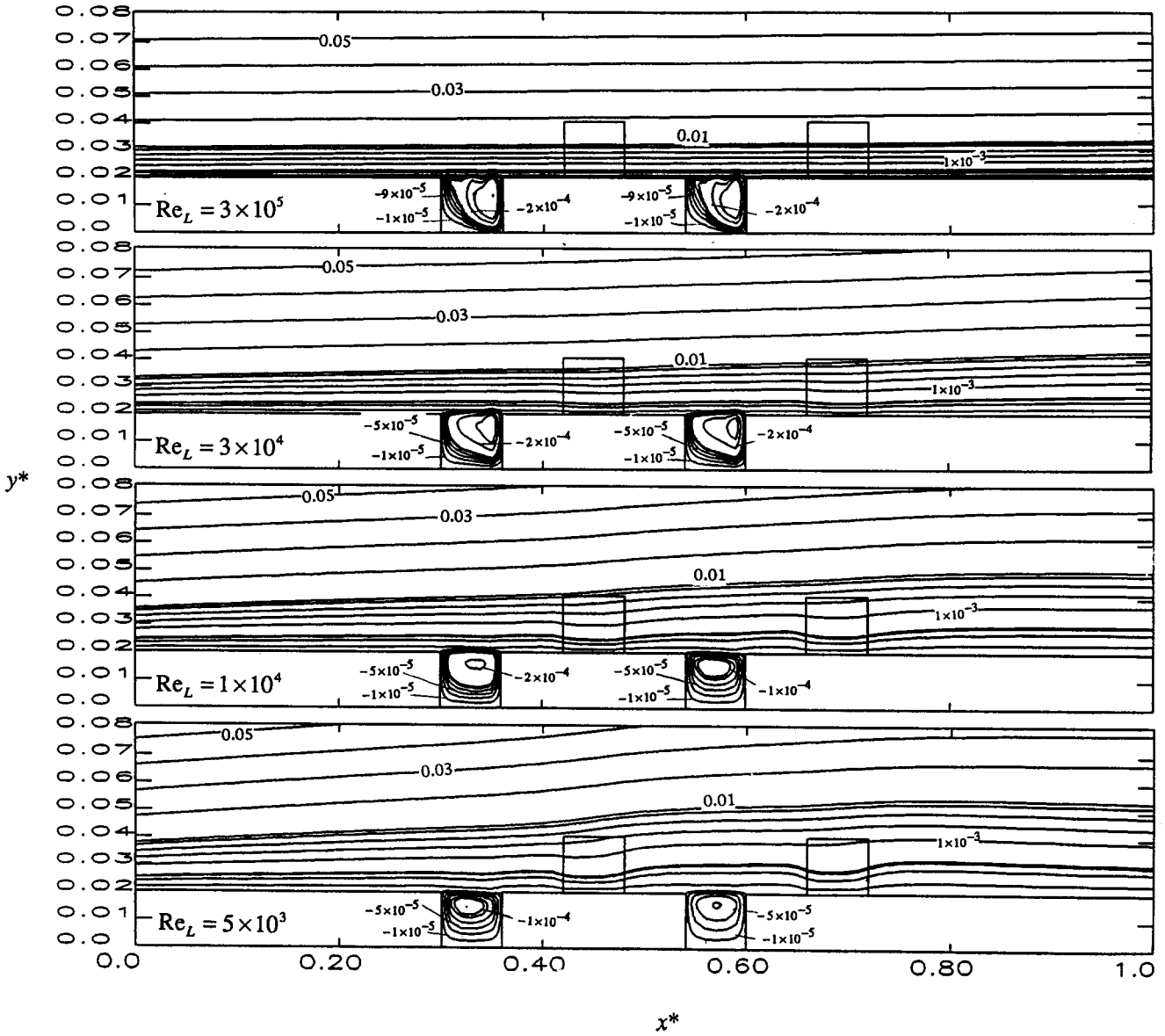

Figure 7 Effects of the Reynolds number on streamlines for flow through alternate porous cavity-block obstacles for $Da_L = 8 \times 10^{-6}$, $\Lambda_L = 0.35$, $A = 3$, $B = 1$, $H^* = 0.02$

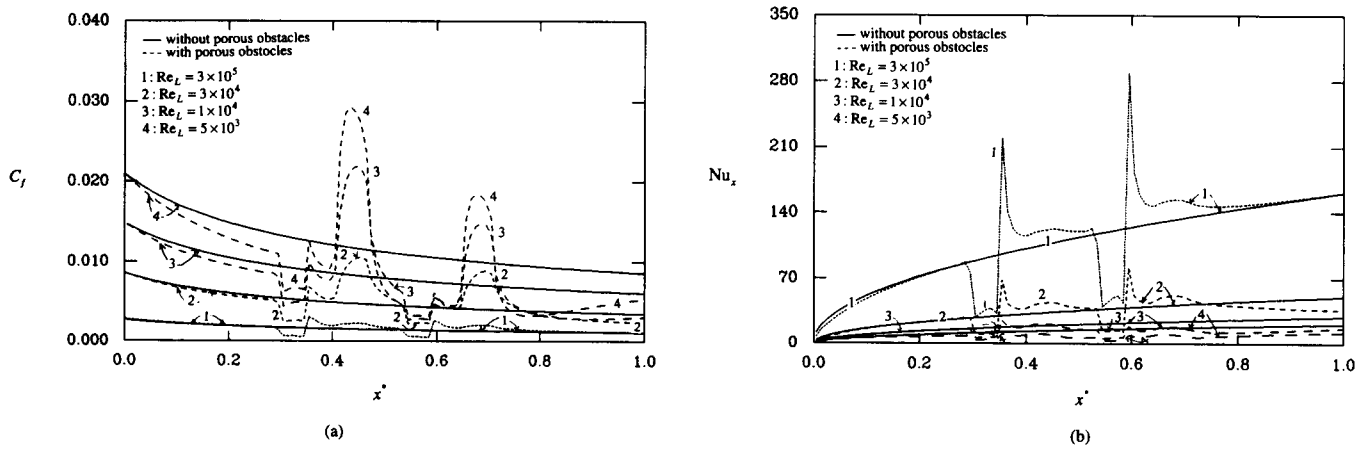

Figure 8 Effects of the Reynolds number on (a) friction coefficient and (b) Nusselt number for flow through alternate porous cavity-block obstacles for $Da_L = 8 \times 10^{-6}$, $\Lambda_L = 0.35$, $Pr = 0.7$, $k_{eff}/k_f = 1.0$, $A = 3$, $B = 1$, $H^* = 0.02$

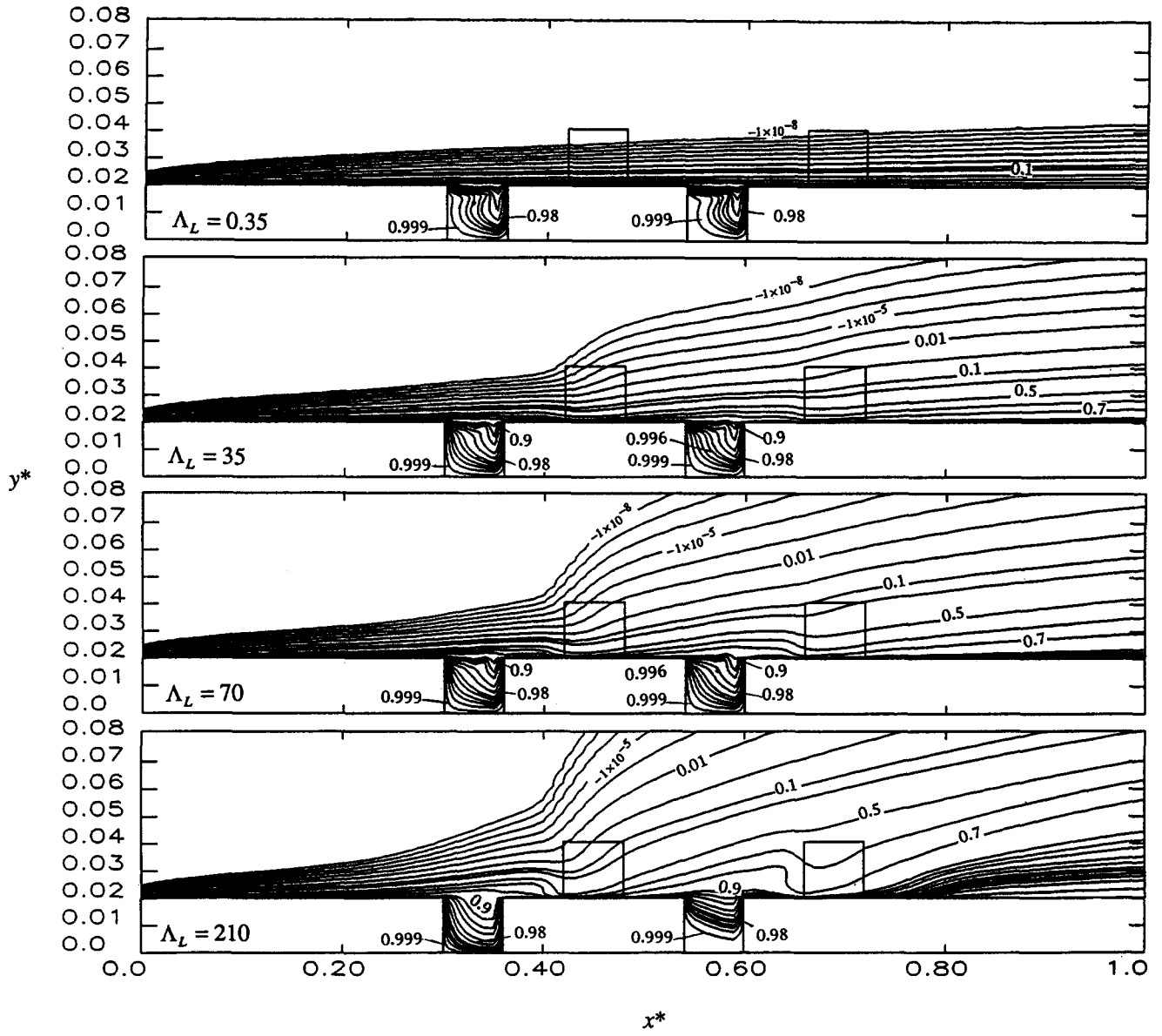

Figure 9 The influence of the inertial parameter on streamlines for flow through alternate porous cavity-block obstacles for $Re_L = 3 \times 10^5$, $Da_L = 8 \times 10^{-6}$, $A = 3$, $B = 1$, $H^* = 0.02$

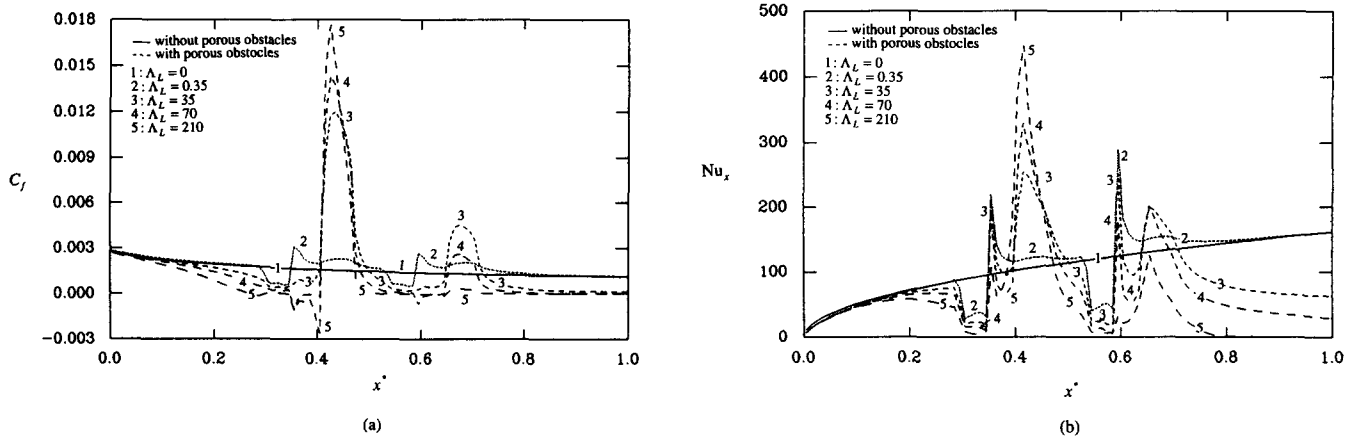

Figure 10 The influence of the inertial parameter on (a) friction coefficient and (b) Nusselt number for flow through alternate porous cavity-block obstacles for $Re_L = 3 \times 10^5$, $Da_L = 8 \times 10^{-6}$, $Pr = 0.7$, $k_{eff}/k_f = 1.0$, $A = 3$, $B = 1$, $H^* = 0.02$

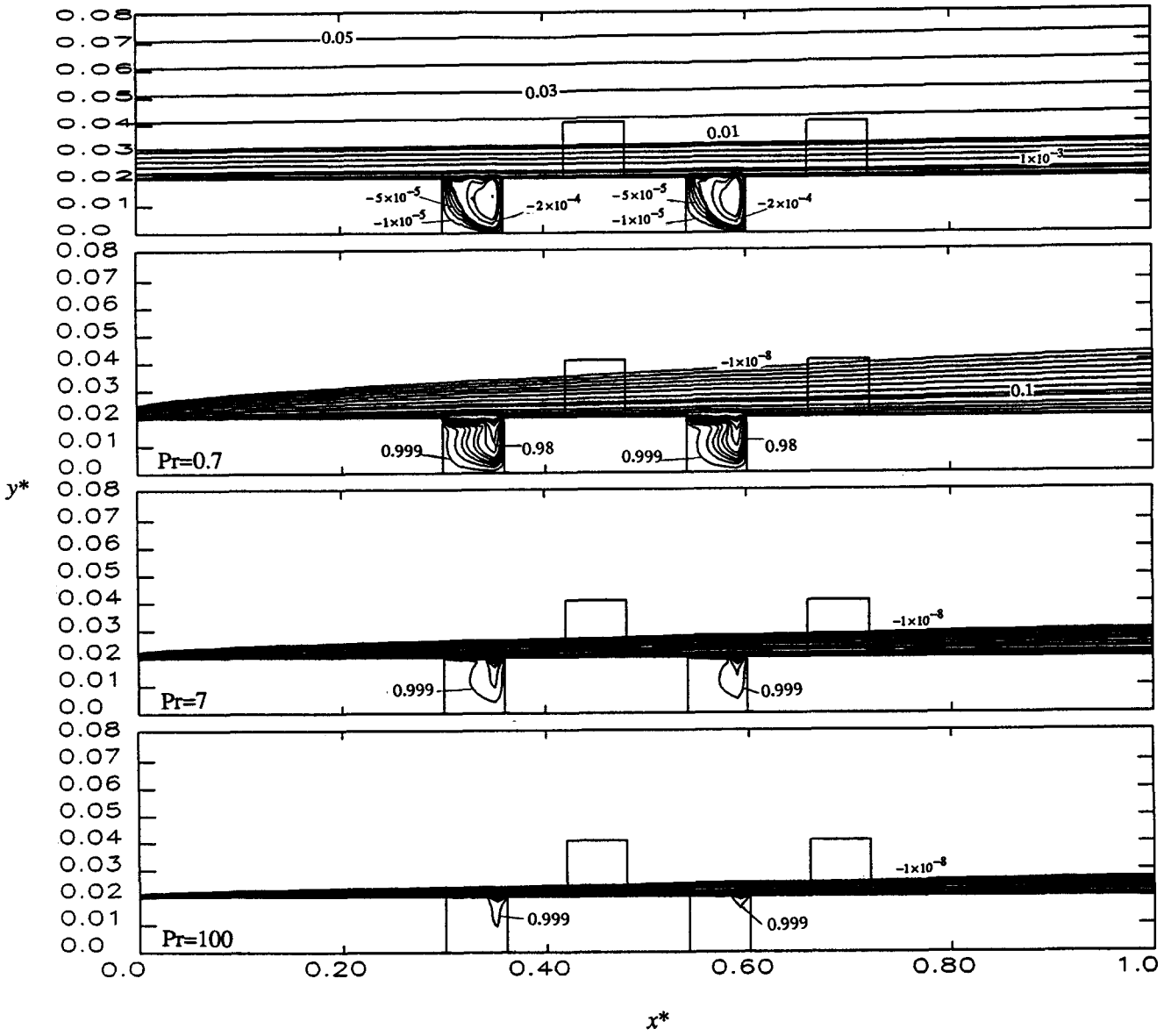

Figure 11 Prandtl number effects on streamlines for flow through alternate porous cavity-block obstacles for $Re_L = 3 \times 10^5$, $Da_L = 8 \times 10^{-6}$, $\Lambda_L = 0.35$, $k_{eff}/k_f = 1.0$, $A = 3$, $B = 1$, $H^* = 0.02$

corresponded to $Re_L = 3 \times 10^5$, $Da_L = 2 \times 10^{-7}$, $\Lambda_L = 0.35$, $Pr = 0.7$, and $A = 3$ for $B = 1$ and 2. The streamlines and isotherms for these cases are also presented in Figures 13 and 14, respectively. As can be seen, when the value of B increases from 1 to 2, the distortions of streamlines and isotherms as well as the effect of boundary layer separation zone on the recirculating flow inside the cavity become less pronounced. This is due to the larger interspacing between porous cavities and blocks, which delays the blowing and deceleration actions.

Effects of larger set of porous cavity block configurations

The effects of larger set of porous cavity block configurations are shown in Figure 15. This figure displays the results for the external flow over three porous cavity-block structures with $A = 3$ and $B = 1$ for $Re_L = 3 \times 10^5$, $Da_L = 2 \times 10^{-7}$, $\Lambda_L = 0.35$, $Pr = 0.7$. As can be seen in this figure the increase in the

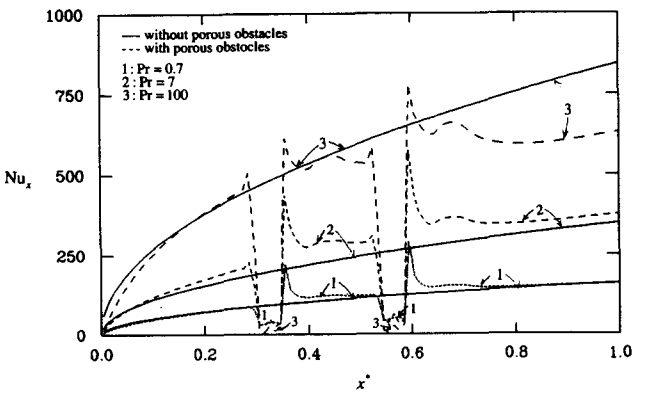

Figure 12 Prandtl number effects on Nusselt number for flow through alternate porous cavity-block obstacles for $Re_L = 3 \times 10^5$, $Da_L = 8 \times 10^{-6}$, $\Lambda_L = 0.35$, $k_{eff}/k_f = 1.0$, $A = 3$, $B = 1$, $H^* = 0.02$

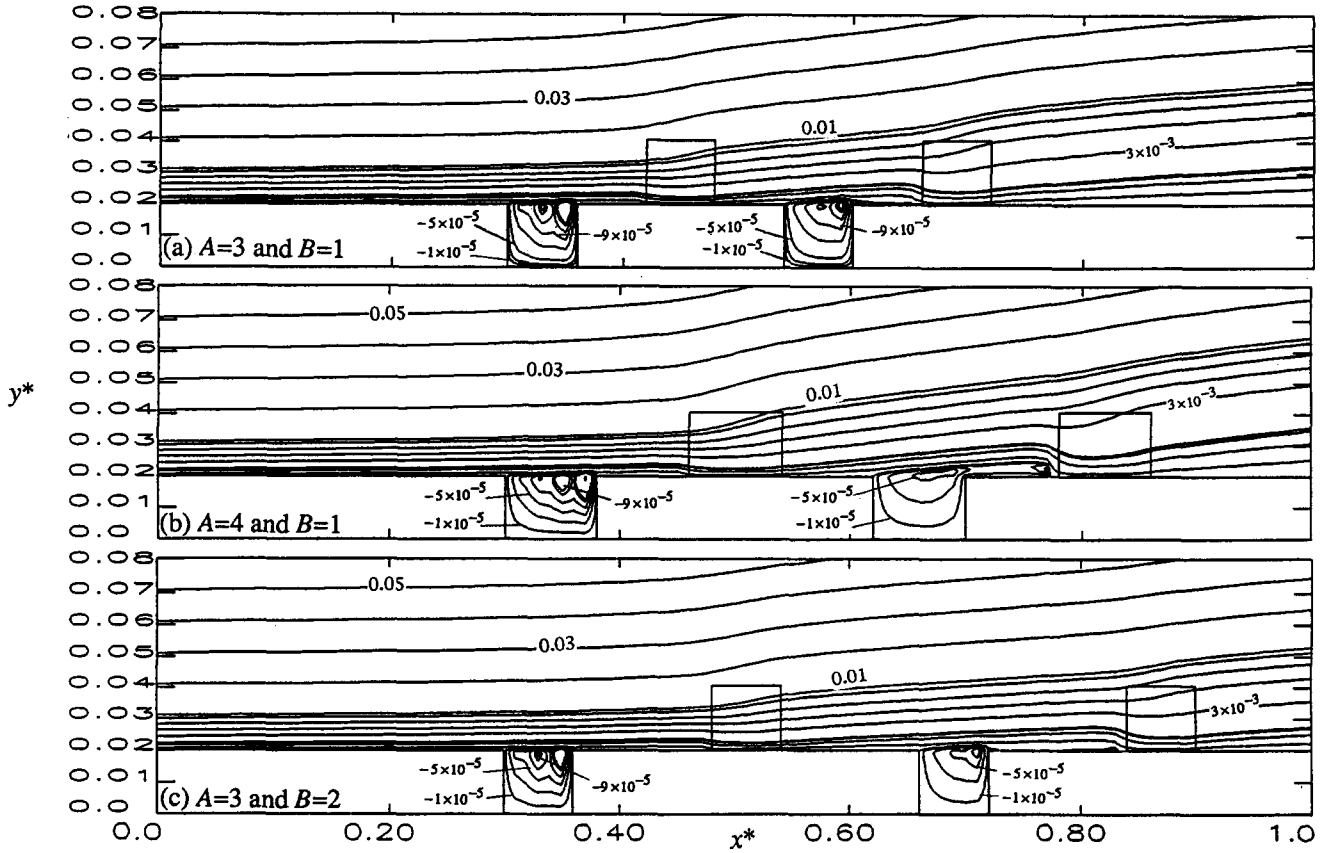

Figure 13 The influence of the geometrical layout on streamlines for flow through alternate porous cavity-block obstacles for $Re_L = 3 \times 10^5$, $Da_L = 2 \times 10^{-7}$, $\Lambda_L = 0.35$, $k_{eff}/k_f = 1.0$, Pr = 0.7, $H^* = 0.02$ at (a) $A = 3$, $B = 1$; (b) $A = 4$ and $B = 1$; and (c) $A = 3$ and $B = 2$

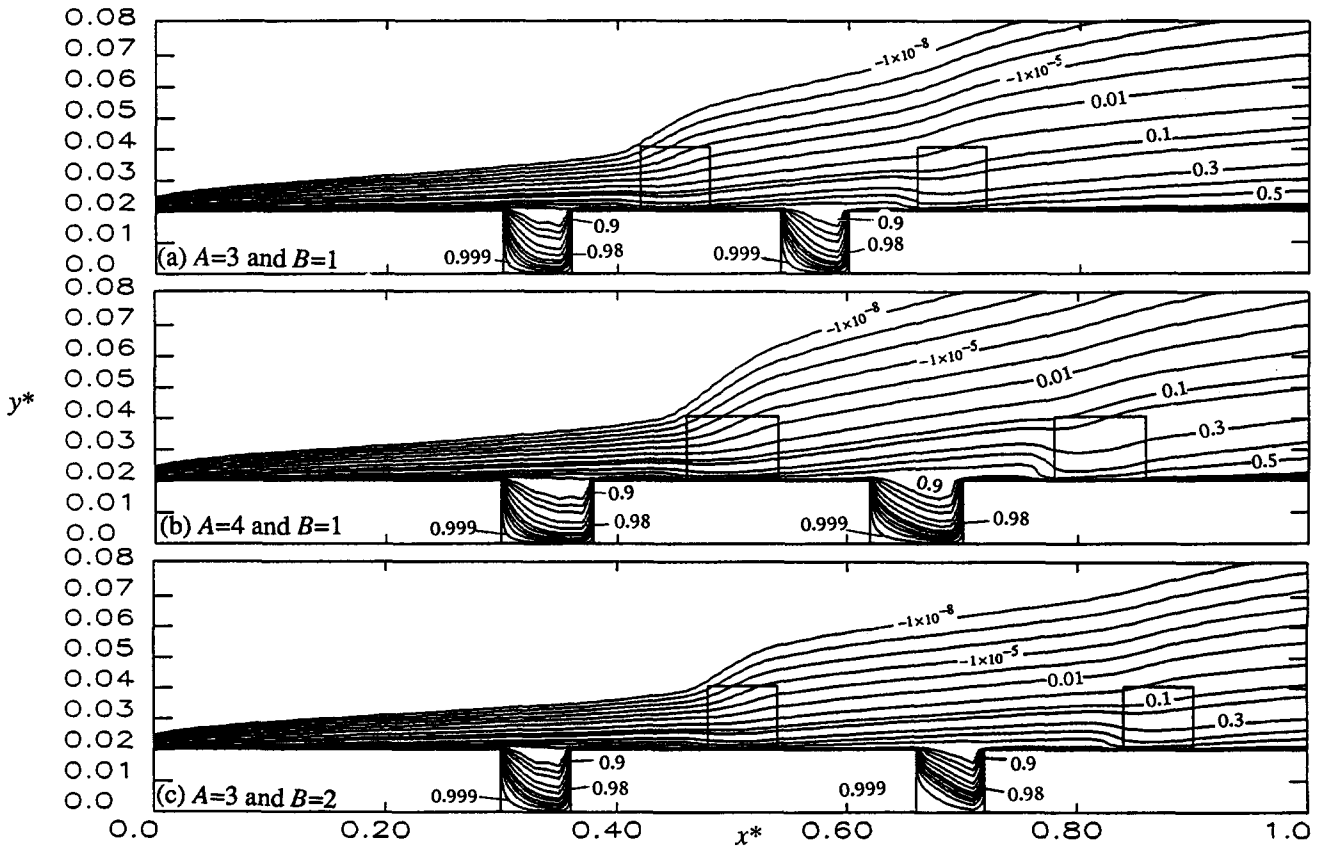

Figure 14 The influence of the geometrical layout on isotherms for flow through alternate porous cavity-block obstacles for $Re_L = 3 \times 10^5$, $Da_L = 2 \times 10^{-7}$, $\Lambda_L = 0.35$, $k_{eff}/k_f = 1.0$, Pr = 0.7, $H^* = 0.02$ at (a) $A = 3$, $B = 1$; (b) $A = 4$ and $B = 1$; and (c) $A = 3$ and $B = 2$

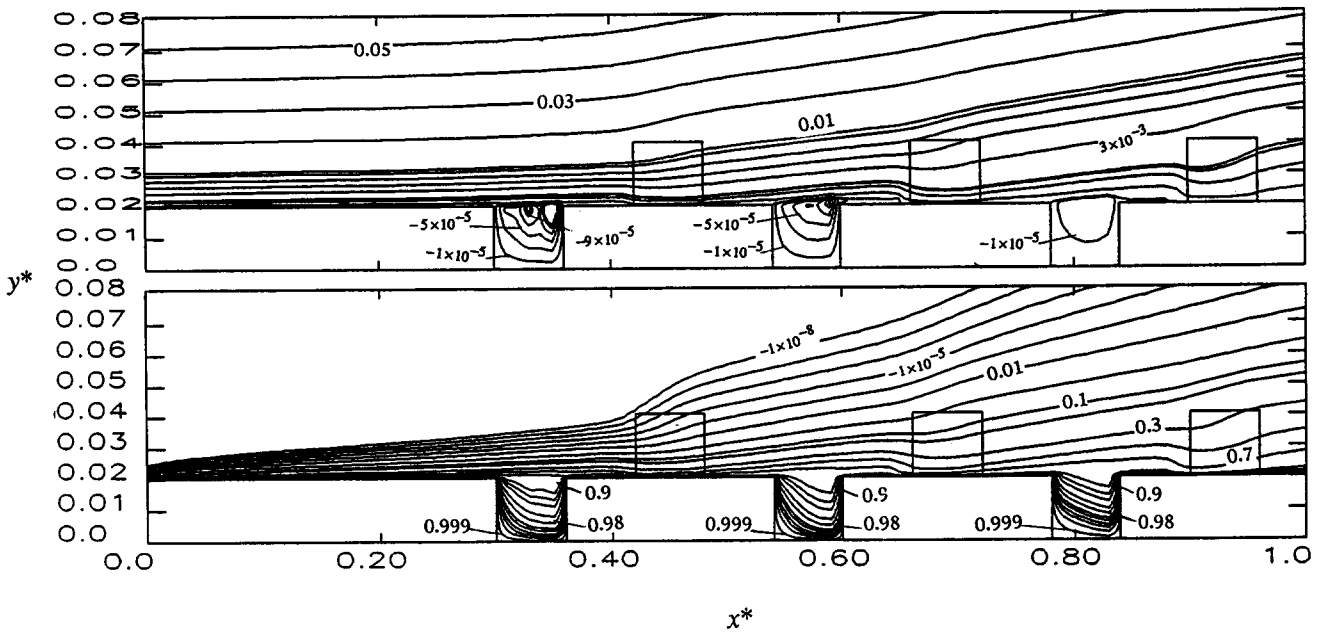

Figure 15 Effects of larger set of porous cavity block configurations: (a) streamlines and (b) isotherms for $Re_L = 3 \times 10^5$, $Da_L = 2 \times 10^{-7}$, $\Lambda_L = 0.35$, $k_{eff}/k_f = 1.0$, Pr = 0.7, $A = 3$, $B = 1$, $H^* = 0.02$, N = 3

number of cavity-block obstacles does not alter the main features of the flow and temperature fields.

Conclusion

Passive control and alteration of heat transfer using alternate porous cavity-block wafers has been presented in this work. The effects of all of the governing parameters such as the Darcy number, Reynolds number, inertia parameter, Prandtl number, the two geometric parameters, and the number of cavity-block structures on the flow and temperature fields were explored in detail. The present work constitutes an innovative way of altering and control of the flow and heat transfer characteristics of an external surface. Throughout the study a reasonably wide range of the independent parameters were covered. An in-depth discussion of the results for various physical interactions between the recirculating flows inside of the cavity and the external flow was presented. Several interesting phenomena such as the interactions between the blowing and displacement effects from the porous blocks and the vortices penetrating into the porous cavities were presented and discussed. These results indicate that altering some parametric values can have significant effects on the external momentum and thermal boundary-layer characteristics. The present investigation forms a pertinent and basic research investigation for altering the skin friction and heat-transfer characteristics of an external surface.

References

Adams, J. and Ortega, J. A. 1982. Multicolor SOR method for parallel computation. *Proc. Int. Conf. on Parallel Procession*, 53–56

Aung, W. and Watkins, C. B. 1979. Heat transfer mechanisms in separated forced convection. *Proc. NATO Institute on Turbulent Forced Convection in Channels and Rod Bundles*

Beavers, G. I. and Joseph, D. D. 1967. Boundary conditions at a naturally permeable wall. *J. Fluid Mech.*, **30**, 197–207

Fletcher, L. S., Briggs, D. G. and Page, R. H. 1974. Heat transfer in separated and reattached flow: an annotated review. *Israel J. Tech.*, **12**, 236–261

Greenspan, D. 1969. Numerical studies of steady, viscous, incompressible flow in a channel with a step. *J. Eng. Mathematics*, **3** (1), 21–28

Huang, P. C. and Vafai, K. 1993. Flow and heat transfer control over an external surface using a porous block array arrangement. *Int. J. Heat Mass Transfer*, **36**, 4019–4032

Kaviany, M. 1987. Boundary layer treatment of forced convection heat transfer from a semi-infinite flat plate embedded in porous media. *Trans. ASME, J. Heat Transfer*, **109**, 345–349

Lauriat, G. and Vafai, K. 1991. *Forced Convective Flow and Heat Transfer Through a Porous Medium Exposed to a Flat Plate or a Channel.* Kluwer Academic Publishers, New York, 289–328

Levy, T. and Sanchez-Palencia, E. 1975. On boundary conditions for fluid flow in porous media. *Int. J. Eng Sci.*, **13**, 923–940

Lundgren, T. S. 1972. Slow flow through stationary random beds and suspensions of spheres. *J. Fluid Mech.*, **51**, 273–299

Neale, G. and Nader, W. 1984. Practical significance of Brinkman's extension of Darcy's law: coupled parallel flows within a channel and a bounding porous medium. *Can. J. Chem. Eng.*, **52**, 475–478

Patankar, S. V. 1980. Numerical heat transfer and fluid flow. Hemisphere, New York

Poulikakos, D. and Kazmierczak, K. M. 1987. Forced convection in a duct partially filled with a porous material. *J. Heat Transfer*, **109**, 653–662

Roache, P. J. 1982. *Computational Fluid Dynamics*, Hermosa

Tien, C. L. and Vafai, K. 1989. Convective and radiative heat transfer in porous media. *Adv. Appl. Mech.*, **27**, 225–282

Vafai, K. and Kim, S. J. 1990. Analysis of surface enhancement by porous substrate. *Trans. ASME*, **112**, 700–705

Vafai, K. and Thiyagaraja, R. 1987. Analysis of flow and heat transfer at the interface region of a porous medium. *Int. J. Heat Mass Transfer*, **30**, 1391–1405

Vafai, K. and Tien, C. L. 1981. Boundary and inertia effects on flow and heat transfer in porous media. *Int. J. Heat Mass Transfer*, **24**, 195–203